Active robust control for wing vibrations attenuation

Ioan URSU[1], Adrian TOADER*,[1], Daniela ENCIU[1], George TECUCEANU[2]

*Corresponding author
[1]INCAS – National Institute for Aerospace Research "Elie Carafoli",
B-dul Iuliu Maniu 220, Bucharest 061126, Romania,
ursu.ioan@incas.ro, toader.adrian@incas.ro*, enciu.daniela@incas.ro
[2]Aerospace Consulting,
B-dul Iuliu Maniu 220, Bucharest 061126, Romania,
tecuceanu.george@incas.ro

DOI: 10.13111/2066-8201.2022.14.1.17

Received: 14 December 2021/ Accepted: 02 Februarie 2022/ Published: March 2022

Abstract: *In this paper a flexible smart wing is presented. The aileron wing with aileron was tested in the INCAS Subsonic Wind Tunnel with the aim of flutter mitigation and vibrations attenuation. The work takes over some of the results of the active anti-flutter control tests performed in the wind tunnel based on the receptance method. More specifically, the mathematical models in the time domain, necessary for the synthesis of control laws, are obtained from experimentally identified transfer functions. The main part of the paper presents the synthesis and analysis of the robustness of the control laws LQG, LQG/LTR, H_∞ standard and H_∞ robust from which the optimal solution will be chosen in a later work for the active vibration control tests on this smart wing model.*

Key Words: *smart wing, robust active control, H_∞ synthesis, Linear Quadratic Gaussian (LQG) synthesis, LQG/LTR (Loop Transfer Recovery) synthesis, flutter mitigation, vibrations attenuation*

1. INTRODUCTION

The application of green technology in aviation requires, among other things, the achievement of light and flexible aircraft, see https://www.tandemaerodays19-20.eu/presentations/. A dialectics of opposites shows however that having a flexible and light aircraft from the perspective of green aviation requirements unfortunately means having a vulnerability in terms of the aircraft's sensitivity to structural vibration regimes and harmfully dynamic stresses. The vibrations, getting more dangerous as they increase in intensity and duration, reach a disastrous level that causes the structure to break. From a mechanical point of view, this occurs when the aerodynamic, elastic, and inertial forces are not balanced, the structure entering a region of dynamic aero (servo) elastic instability characterized by self-sustained oscillations whose amplitudes increase rapidly. This destructive phenomenon is called flutter.

There is also a risk that cannot be neglected, that of flutter triggering if the impedance (alike called "dynamic stiffness") of the hydraulic servomechanism in the control chain has a negative damping [1-3]. The aeroservoelastic compatibility of the hydraulic servomechanism used in the primary flight controls of the aircraft IAR-93 Eagle was analysed, based on the hydraulic servomechanism impedance concept in [4]. The result of the analysis highlighted a negative dynamic stiffness of the servomechanism retrieved from aircraft MIG 21 out of use, so the report gave a negative vote on its aeroservoelastic compatibility in the control chain of

the aircraft being designed and built. Sadly, this result was ignored by the decision makers from that time, given the lack of specific requirements about impedance in the Aviation Publication (AvP) 970 dated 1959. On November 24 1977, an IAR-93 Eagle ground attack and tactical reconnaissance aircraft crashed as a result of the left elevator broke off due to flutter (see https://en.wikipedia.org/wiki/IAR-93_Vultur). (As an irony of fate, the requirement on the positive dynamic stiffness of the impedance function of the hydraulic servomechanisms from the primary flight controls has been introduced, a few years later, in the updated version of that Regulation). That catastrophe of 1977 eventually led to the replacement of the initial hydraulic servomechanisms of the flight controls, which were improper from an aeroservoelastic point of view, with hydraulic servomechanisms manufactured in collaboration with the Dowty Group (https://en.wikipedia.org/wiki/Dowty_Group).

There is a large bibliography regarding the active control of the vibrations and flutter of the aircraft in general, the influence of servo actuators, the gust loads and gust loads alleviation, the active control techniques, the programs and tests in the wind tunnel, etc. An exceptional state of the art and technology in this field gives us the paper [5], which the interested reader can confidently appeal to. From there we learned that "the first active flutter suppression system to fly on a production airplane was probably that of the F-18" [6], being in fact a Limit-Cycle Oscillation control system. Since then, from 1985 until today, research and applications of active control have continued, with new approaches and achievements.

This paper is an intermediate stage in a slightly larger research on the development of an active vibration control demonstrator – a wing with aileron – tested in the Wind Tunnel (WT). A first stage already completed was the conception of a piezoelectric actuator and the application of the receptance method, which has two components: the experimental identification of the mathematical model of the wing and the synthesis of control [7-10]. The tests in INCAS subsonic WT [8-11] showed a significant attenuation of the vibrations, thus validating the receptance method. In this context, the subject of research in the present paper is a rather theoretical study, preparatory for a later stage of testing in WT, namely the development and verification by numerical simulation of some robust control laws.

Therefore, Section 2 presents a review of some robust control laws − LQG/LTR and H_∞ Robust control laws are validated by numerical simulations in Section 3, which also contains some conclusions on the analysed methodology.

2. REVIEW OF SOME ROBUST ACTIVE CONTROL LAWS FOR VIBRATIONS ATTENUATION

2.1 Experimental identification of structural mathematical model of the wing

Counteracting vibrations and flutter is a priority in aeroservoelasticity studies. The servo actuators, whether those of flight controls, or special implemented servo actuators, are directly involved in vibration and flutter "management". As mentioned in the previous chapter, a piezoelectric V-stack servoactuator was developed to drive the aileron of the wing model [10]. The piezoelectric stacks were chosen due to their advantages like small size and large bandwidth (**Figure 1**).

The disadvantage of piezo stacks low strokes was compensated by the kinematics choice [10]. In this way, a maximum stroke of 148.8 μm of the piezo stack was increased at about 1300 μm at the point of application of a 460 N active force to a first-order lever that defines the aileron with its deflection.

The wing model was specially designed to create a realistic, elastic wing, unlike most rigid models with external springs simulating elasticity, as found in literature [12-13].

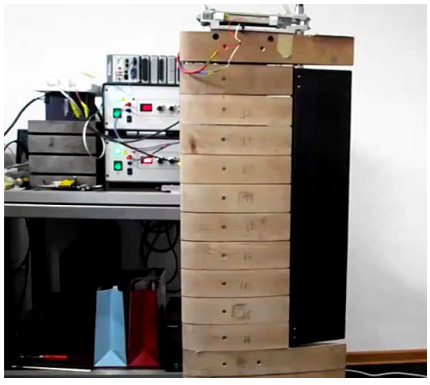

Figure 1 – From left to right: wing with aileron, piezoactuator and two accelerometers; wing in WT

The demonstrator, consisting of the wing with aileron and piezo actuator, was set-up in the subsonic WT for tests at several air velocities with the purpose of flutter speed identification in the absence of a control law. The results indicated that the flutter speed was 41 m/s and the flutter frequency was 5.8 Hz. The natural frequencies of the specimen were measured in the Mechatronics Laboratory of INCAS: 5.865 Hz (bending), 14.463 Hz (torsion), 23.137 Hz, 41.850 Hz, 49.413 Hz [8-9].

Two problems must be solved in the case of the control law synthesis: that of mathematical modelling of the controlled system and that of compatibility between a mathematical methodology intended to be used for control law synthesis and the mathematical model to which this methodology is applied [14]. If necessary, the second problem is usually solved by adapting the mathematical model, benefiting from its flexibility. For mathematical modelling of the system, the conventional approach follows an analytical path, [15] or a numerical one, by using finite element method (FEM) [16-18]. This time, the determination of a structural mathematical model was performed by online identification, considered more secure than any analytical or FEM approach, especially in this particular case of the wing having an atypical longeron. Therefore, the receptance method for the active control synthesis was used [7-10]. From the receptance method, we retain the experimental identification procedure that we detail here. Briefly described, the active control law synthesis requires the identification of the open loop transfer functions, $H_{y_{iu}}(s),\ i = 1, 2,$ from a chirp signal applied to the piezo actuator to the two accelerometers placed on the wing (**Figure 1**, on the right), the first located near the leading edge and the second located near the wing axis. The identification procedure takes place in the mounting set-up shown in **Figure 1** on the right, at some air speeds, and is sequentially carried out as follows: **a)** a chirp signal $\delta_c(t)$ is applied to the piezoactuator; the signal has constant amplitude (corresponding to an expected angular aileron displacement, for example 2 degrees, 4 degrees, etc.) and linearly variable frequency in time in the band [0 Hz; 60 Hz], which sufficiently covers the interest field of the first two modal frequencies of the wing (this is because we took only the first two frequencies as the objective of the vibration damping process); **b)** the normal acceleration signal at the wing surface is integrated twice to obtain the displacements $y_i(t)$; the accelerometers are mounted on the wing so as to react to bending and torsional movements corresponding to the first three modes of vibration, respectively;

c) the **exp**erimental frequency response, defined by the $\left|H_{y_i\delta_c,\mathbf{exp}}(i\omega_j)\right|, i = 1,2$ – attenuation-frequency characteristics, and $\arctan\left(\mathrm{Im}\left(H_{y_i\delta_c,\mathbf{exp}}(i\omega_j)\right)/\mathrm{Re}\left(H_{y_i\delta_c,\mathbf{exp}}(i\omega_j)\right)\right), i = 1,2$ – phase-frequency characteristics, $j = 1,\ldots,M$, $i = \sqrt{-1}$, associated with the transfer function $H_{y\delta_c;exp}(i\omega)$ is estimated; the latter is obtained by comparing (dividing) the Fast Fourier Transform (FFT) of the two experimental time signals $y(t)$ and $\delta_c(t)$; therefore, $H_{y_i\delta_c;\mathbf{exp}}(i\omega), i = 1,2$ consists of a sequence of complex numbers, of length M, indexed with values of the circular frequencies ω_j; **d)** a convenient approximation of this response by rational transfer functions is sought (i.e., a ratio of two polynomials in the complex variable $s = i\omega$), $H_{y_i\delta_c;\mathbf{idt}}(i\omega) \cong H_{y_i\delta_c;\mathrm{exp}}(i\omega)$; for this purpose, functions from the MATLAB System **Id**en**t**ification Toolbox are available.

Four air velocities were chosen: V_1 = 15 m/s; V_2 = 20 m/s; V_3 = 25 m/s; V_4 = 30 m/s. The number of poles and zeros corresponding to the four air velocities in WT (see Table 1) were determined using MATLAB so that the frequency responses $H_{y_iu}(i\omega)$ approximates the experimental ones, as well as possible. Since the control synthesis aimed at attenuating the first vibration mode, only the transfer functions $H_{y_1u}(i\omega)$ were used.

State space realizations $(\widetilde{\boldsymbol{A}}, \widetilde{\boldsymbol{B}}_2, \widetilde{\boldsymbol{C}}_2, 0)$ were obtained using the MATLAB subroutine `tf2ss`, for each of the four transfer functions. Further processing was done to bring the state matrix to the modal form:

$$\boldsymbol{A} = \begin{bmatrix} \mathbf{0}_{3\times3} & \mathbf{I}_3 \\ \boldsymbol{diag}(-\omega_i^2) & \boldsymbol{diag}(-2\zeta_i\omega_i) \end{bmatrix},\ i = \overline{1,3}. \tag{1}$$

Obviously, the equivalent input-to-state matrix $\boldsymbol{B}_2$ and state-to-output matrix $\boldsymbol{C}_2 = [1\ \ 1\ \ 1\ \ 0\ \ 0\ \ 0]$ are obtained. Thus, the synthesis of the control laws starts from the four triplets of matrices$(\boldsymbol{A}, \boldsymbol{B}_2, \boldsymbol{C}_2)$.

Table 1 – Transfer function $H_{y_1u}(i\omega)$ for various air velocities

Air velocity [m/s]	Poles	Zeros	Frequency $\boldsymbol{\omega_i}$ [Hz]	Damping ratio $\boldsymbol{\zeta_i}$
15	-0.74 ± 36.74i	4602.5	5.85	0.02
	-6.21± 95.39i	111.5	15.21	0.07
	-51.85 ± 178.36i	-28.9 ± 48.3i	29.56	0.28
20	-1.13 ±37.19i	294.2	5.92	0.03
	-7.70 ± 95.46i	159.75	15.24	0.08
	-80.95 ± 202.83i	-31.65 ± 51.2i	34.76	0.37
25	-1.34 ± 37.55i	-3064.4	5.98	0.03
	-10.63 ± 94.90i	99.4	15.20	0.11
	-59.80 ± 184.28i	63.4 ± 53.7i	30.83	0.31
30	-1.69 ± 37.73i	1643.3	6.01	0.05
	-13.92 ± 93.95i	-407.6	15.12	0.15
	-81.45 ± 216.13i	126.6; -58.3	36.76	0.35

2.2 Robust active control laws

For the synthesis of the control laws, the robust techniques LQG/LTR and H_∞ were chosen for two reasons: firstly, to highlight in applications the increase of vibration attenuation performance compared to LQG and standard H_∞ techniques, respectively, and secondly, to compare them with each other, see also works [17], [18].

Standard LQG control synthesis

The matrix $\boldsymbol{A}$ (1) is associated with second order structural models:

$$\ddot{\boldsymbol{q}} + \boldsymbol{diag}\left(2\zeta_i\omega_i\right)\dot{\boldsymbol{q}} + \boldsymbol{diag}(\omega_i^2)\boldsymbol{q} = \boldsymbol{B}_1\xi + \boldsymbol{B}_2 u \tag{2}$$

for $i = 1,2,3$, in which a Gaussian component $\boldsymbol{B}_1\xi$ of the aerodynamic turbulence perturbation was considered. These models were used as a basis for the control laws synthesis in the framework of LQG standard optimal problem [19]:

$$\dot{\boldsymbol{x}}(t) = \boldsymbol{A}\boldsymbol{x}(t) + \boldsymbol{B}_1\xi(t) + \boldsymbol{B}_2(t)u(t);\ z(t) = \boldsymbol{C}_1\boldsymbol{x}(t), y(t) = \boldsymbol{C}_2\boldsymbol{x}(t) + \mu\eta(t) \tag{3}$$

where $\boldsymbol{x}(t)$ is the state, $z(t)$ is the quality output, with $\boldsymbol{C}_1 = \boldsymbol{C}_2$, $y(t)$ is the measured output, and $u(t)$ is the control input. The state vector is given by the displacements and velocities of the three modes highlighted in (1):

$$\boldsymbol{x}(t) = (q_3\,, q_2\,, q_1\,, \dot{q}_3\,, \dot{q}_2\,, \dot{q}_1\,)^{\mathrm{T}}. \tag{4}$$

$\xi(t)$ and $\eta(t)$ are white noises on state and measured output, $\boldsymbol{B}_1 = \boldsymbol{B}_2$ respectively, since noise and control are considered to operate at the same point in the system. The exponent "T" stands for the transpose of a matrix or vector. The objective is to find the control law $u(t)$ which stabilizes the system (3) and minimizes the cost function.

$$J_{LQG} = \lim_{T\to\infty} \mathrm{E}\left\{\int_0^T \begin{bmatrix}\boldsymbol{x}(t)^{\mathrm{T}} & u(t)^{\mathrm{T}}\end{bmatrix}\begin{bmatrix}\boldsymbol{Q} & 0\\ 0 & R\end{bmatrix}\begin{bmatrix}\boldsymbol{x}(t)\\ u(t)\end{bmatrix} dt\right\} \tag{5}$$

with $\boldsymbol{Q} = \boldsymbol{C}_1^{\mathrm{T}}\boldsymbol{Q}_J\boldsymbol{C}_1$. $\boldsymbol{Q}_J$ and R are weights and herein R is scalar. Cost function is thought as a trade-off between the quality output $z(t)$ and control $u(t)$ trade-off, thus ensuring an active realistic vibration mitigation. The solution refers to the development of a controller and a state-estimator, e.g., a Kalman filter [20]. The state estimator is described by:

$$\dot{\hat{\boldsymbol{x}}} = \boldsymbol{A}\hat{\boldsymbol{x}}(t) + \boldsymbol{B}_2 u + \boldsymbol{K}_f\left(y(t) - \boldsymbol{C}_2\hat{\boldsymbol{x}}(t)\right). \tag{6}$$

The controller is given by:

$$u(t) = -\boldsymbol{K}_R\hat{\boldsymbol{x}}(t). \tag{7}$$

The LQG control is obtained by solving the decoupled algebraic Riccati equations

$$\boldsymbol{A}^{\mathrm{T}}\boldsymbol{P} + \boldsymbol{P}\boldsymbol{A} - \boldsymbol{P}\boldsymbol{B}_2R^{-1}\boldsymbol{B}_2^{\mathrm{T}}\boldsymbol{P} + \boldsymbol{C}_1^{\mathrm{T}}\boldsymbol{Q}_J\boldsymbol{C}_1 = 0, \boldsymbol{A}\boldsymbol{S} + \boldsymbol{S}\boldsymbol{A}^{\mathrm{T}} - \boldsymbol{S}\boldsymbol{C}_2^{\mathrm{T}}Q_\eta^{-1}\boldsymbol{C}_2\boldsymbol{S} + \boldsymbol{B}_1Q_\xi\boldsymbol{B}_1^{\mathrm{T}} = 0 \tag{8}$$

with the noise matrices Q_ξ and Q_η described by:

$$\mathrm{E}\left\{\begin{bmatrix}\xi(t)\\ \eta(t)\end{bmatrix}[\xi(t) \quad \eta(t)]\right\} = \begin{bmatrix}Q_\xi & 0\\ 0 & Q_\eta\end{bmatrix}\delta(t-\tau) \tag{9}$$

where $\delta(t-\tau)$ is the Dirac distribution. Substituting the controller (7) in the first equation (3) and in (6), we obtain the closed loop system:

$$\begin{aligned}\dot{\boldsymbol{x}}(t) &= \boldsymbol{A}\boldsymbol{x}(t) + \boldsymbol{B}_1\xi(t) - \boldsymbol{B}_2\boldsymbol{K}_R\hat{\boldsymbol{x}}(t)\\ \dot{\hat{\boldsymbol{x}}}(t) &= \boldsymbol{K}_f C_2 x(t) + \boldsymbol{K}_f\mu\boldsymbol{I}\eta(t) + \left(\boldsymbol{A}_2 - \boldsymbol{B}_2\boldsymbol{K}_R - \boldsymbol{K}_f\boldsymbol{C}_2\right)\hat{\boldsymbol{x}}(t)\end{aligned} \tag{10}$$

$\boldsymbol{K}_R$ and $\boldsymbol{K}_f$ are given by the solutions of the Riccati equations (8):

$$\boldsymbol{K}_R = R^{-1}\boldsymbol{B}_2^{\mathrm{T}}\boldsymbol{P}\,, \qquad \boldsymbol{K}_f = \boldsymbol{S}\boldsymbol{C}_2^{\mathrm{T}}Q_\eta^{-1}\,. \tag{11}$$

LQG/LTR control synthesis

In our opinion, the most remarkable achievement in a history of over 80 years of control science is the LQG synthesis since it provides an elegant and realistic control synthesis, being

based on a state estimator, in comparison with the unrealistic LQR (Linear Quadratic Regulator) synthesis, which is based on the illusory knowledge of all the states of the system. Unfortunately, the LQG synthesis is not perfect either, as it does not ensure the robustness of the solution, as does the LQR synthesis [21]. However, this shortcoming was solved within the LQG/LTR synthesis. The mechanism of the LQG/LTR technique is described by some interesting results given in [22].

Proposition 1. *The effect of Kalman filter is the same with the effect of LQR control (with complete state feedback) if the following relation holds:*

$$\boldsymbol{K}_f\left[\boldsymbol{I}+\boldsymbol{C}_2(s\boldsymbol{I}-\boldsymbol{A})\boldsymbol{K}_f\right]^{-1}=\boldsymbol{B}_2[\boldsymbol{C}_2(s\boldsymbol{I}-\boldsymbol{A})^{-1}\boldsymbol{B}_2]^{-1}. \tag{12}$$

Therefore, (12) is the condition of LQR robustness survival in the LQG control.

Proposition 2. *If the Kalman filter gain, parameterized with* $q>0$ *has an asymptotic behaviour* $\boldsymbol{K}_f(q)/q\to\boldsymbol{B_2W}$ *when* $q\to\infty$, $\boldsymbol{W}$ *being a non-singular matrix, then the relation* (12) *holds asymptotically. Such a behaviour can be performed, in the case of a minimum phase system* $(\boldsymbol{C}_2,\boldsymbol{A},\boldsymbol{B}_2)$, *if in the second equation* (8) $\boldsymbol{B}_1Q_\xi\boldsymbol{B}_1^{\mathrm{T}}$ *is substituted by* $\boldsymbol{B}_1Q_\xi\boldsymbol{B}_1^{\mathrm{T}}+q^2\boldsymbol{B}_2\boldsymbol{Q}\boldsymbol{V}\boldsymbol{B}_2^{\mathrm{T}}$ *with* $\boldsymbol{V}>0$ *a symmetrical matrix*.

Definition 1. *The transmission zeros of the system* $\dot{\boldsymbol{x}}(t)=\boldsymbol{A}\boldsymbol{x}(t)+\boldsymbol{B}_2\boldsymbol{u}(t)$, $\boldsymbol{y}(t)=\boldsymbol{C}_2\boldsymbol{x}(t)$, $\boldsymbol{x}\in\mathbb{R}^n$, $\boldsymbol{u}\in\mathbb{R}^p$, $\boldsymbol{y}\in\mathbb{R}^l$ *are complex numbers* s_0 *that satisfy inequality*

$$\operatorname{rank}\begin{bmatrix}\boldsymbol{A}-s_0\boldsymbol{I} & \boldsymbol{B}_2\\ \boldsymbol{C}_2 & \boldsymbol{0}\end{bmatrix}<n+\min(p,l).$$

The given definition assumes that the system$(\boldsymbol{A},\boldsymbol{B}_2,\boldsymbol{C}_2,0)$ is not degenerate [23].

Definition 2. *System* $(\boldsymbol{A},\boldsymbol{B}_2,\boldsymbol{C}_2,\boldsymbol{0})$ *is of minimum phase if its transfer matrix* $\boldsymbol{G}(s):=\frac{\boldsymbol{y}(s)}{\boldsymbol{u}(s)}=\boldsymbol{C}_2(s\boldsymbol{I}-\boldsymbol{A})^{-1}\boldsymbol{B}_2$ *has all zeros in the open left half-plane* [24, 25].

Transfer functions $\boldsymbol{u}'(s)/\boldsymbol{u}(s)$ for cases LQR and LQR/LTR, respectively, are used in Section 3

$$\dot{\boldsymbol{x}}=\boldsymbol{A}\boldsymbol{x}+\boldsymbol{B}_2\boldsymbol{u};\ \boldsymbol{u}'=-\boldsymbol{K}_R\boldsymbol{x};\ \boldsymbol{H}_{\mathrm{LQR}}(s)=\boldsymbol{u}'(s)/\boldsymbol{u}(s)=-\boldsymbol{K}_R(s\boldsymbol{I}-\boldsymbol{A})^{-1}\boldsymbol{B}_2$$

$$\dot{\hat{\boldsymbol{x}}}=\left(\boldsymbol{A}-\boldsymbol{B}_2\boldsymbol{K}_R-\boldsymbol{K}_f\boldsymbol{C}_2\right)\hat{\boldsymbol{x}}+\boldsymbol{K}_f\boldsymbol{C}_2\boldsymbol{x}\Rightarrow\hat{\boldsymbol{x}}(s)=\left[s\boldsymbol{I}-\left(\boldsymbol{A}-\boldsymbol{B}_2\boldsymbol{K}_R-\boldsymbol{K}_f\boldsymbol{C}_2\right)\right]^{-1}\boldsymbol{K}_f\boldsymbol{C}_2\boldsymbol{x}$$

$$\dot{\boldsymbol{x}}=\boldsymbol{A}\boldsymbol{x}+\boldsymbol{B}_2\boldsymbol{u}\Rightarrow\boldsymbol{x}(s)=(s\boldsymbol{I}-\boldsymbol{A})^{-1}\boldsymbol{B}_2\boldsymbol{u};$$

$$\hat{\boldsymbol{x}}(s)=\left[s\boldsymbol{I}-\left(\boldsymbol{A}-\boldsymbol{B}\boldsymbol{K}_R-\boldsymbol{K}_f\boldsymbol{C}_2\right)\right]^{-1}\boldsymbol{K}_f\boldsymbol{C}_2(s\boldsymbol{I}-\boldsymbol{A})^{-1}\boldsymbol{B}_2\boldsymbol{u}$$

$$\boldsymbol{u}'=-\boldsymbol{K}_R\hat{\boldsymbol{x}}=-\boldsymbol{K}_R\left[s\boldsymbol{I}-\left(\boldsymbol{A}-\boldsymbol{B}_2\boldsymbol{K}_R-\boldsymbol{K}_f\boldsymbol{C}_2\right)\right]^{-1}\boldsymbol{K}_f\boldsymbol{C}_2(s\boldsymbol{I}-\boldsymbol{A})^{-1}\boldsymbol{B}_2\boldsymbol{u}$$

$$\boldsymbol{H}_{\mathrm{LQG/LTR}}(s)=\boldsymbol{u}'(\boldsymbol{s})/\boldsymbol{u}(\boldsymbol{s})=-\boldsymbol{K}_R\left[s\boldsymbol{I}-\left(\boldsymbol{A}-\boldsymbol{B}_2\boldsymbol{K}_R-\boldsymbol{K}_f\boldsymbol{C}_2\right)\right]^{-1}\boldsymbol{K}_f\boldsymbol{C}_2(s\boldsymbol{I}-\boldsymbol{A})^{-1}\boldsymbol{B}_2.$$

Another approach of the LQG/LTR technique is that of using the matrices $\boldsymbol{B}_1,\boldsymbol{C}_1$ and the scalars μ and ρ as free parameters in an H_∞-trade-off in which points of interest are the robustness of stability and robustness of performance, characterized by the special functions of sensitivity $\boldsymbol{S}(s)$ and complementary sensitivity $\boldsymbol{T}(s)$ related to Kalman filter gain [26-28]

$$\boldsymbol{S}(s)=\left[\boldsymbol{I}+\boldsymbol{G}(s)\boldsymbol{K}_f(s)\right]^{-1},\qquad\boldsymbol{T}(s)=\boldsymbol{G}(s)\boldsymbol{K}_f(s)\boldsymbol{S}(s). \tag{13}$$

The relevance of these functions derives from the following frequency domain requirements: a) $\boldsymbol{S}(s)$ must be small whenever output perturbations are large and b) $\boldsymbol{T}(s)$ must be small whenever model errors are large.

Standard H_∞ synthesis

Consider the system described in the usual form of the H_∞ synthesis [28]:

$$\begin{gathered}\dot{\boldsymbol{x}}=\boldsymbol{A}\boldsymbol{x}+\boldsymbol{B}_1\boldsymbol{w}+\boldsymbol{B}_2\boldsymbol{u};\ \boldsymbol{z}=\boldsymbol{C}_1\boldsymbol{x}+\boldsymbol{D}_{11}\boldsymbol{w}+\boldsymbol{D}_{12}\boldsymbol{u};\ \boldsymbol{y}=\boldsymbol{C}_2\boldsymbol{x}+\boldsymbol{D}_{21}\boldsymbol{w}+\boldsymbol{D}_{22}\boldsymbol{u};\\ \dot{\hat{\boldsymbol{x}}}=\hat{\boldsymbol{A}}\hat{\boldsymbol{x}}+\hat{\boldsymbol{B}}\boldsymbol{y};\ \boldsymbol{u}=\hat{\boldsymbol{C}}\hat{\boldsymbol{x}}+\hat{\boldsymbol{D}}\boldsymbol{y}\end{gathered} \tag{14}$$

where $\boldsymbol{x} \in \mathbb{R}^n$, $\boldsymbol{w} \in \mathbb{R}^{m_1}$, $\boldsymbol{u} \in \mathbb{R}^{m_2}$, $\boldsymbol{z} \in \mathbb{R}^{p_1}$, $\boldsymbol{y} \in \mathbb{R}^{p_2}$. The left side system represents the plant, and the right one gives the H_∞ controller. Consider the representation of transfer matrix type associated to the nominal system

$$\begin{bmatrix} \boldsymbol{z} \\ \boldsymbol{y} \end{bmatrix} = \begin{bmatrix} \boldsymbol{P}_{11} & \boldsymbol{P}_{12} \\ \boldsymbol{P}_{21} & \boldsymbol{P}_{22} \end{bmatrix} \begin{bmatrix} \boldsymbol{w} \\ \boldsymbol{u} \end{bmatrix}. \tag{15}$$

To apply H_∞ control synthesis, it is necessary to verify that the open-loop plant satisfies several assumptions [28]: the pairs $(\boldsymbol{A}, \boldsymbol{B_2})$, $\left(\widehat{\boldsymbol{A}}, \widehat{\boldsymbol{B}}\right)$ are stabilizable and $(\boldsymbol{C_2}, \boldsymbol{A})$, $\left(\widehat{\boldsymbol{C}}, \widehat{\boldsymbol{A}}\right)$ are detectable; $\boldsymbol{D}_{11}^{\mathrm{T}}[\boldsymbol{C}_1 \quad \boldsymbol{D}_{12}] = [\boldsymbol{0} \quad \boldsymbol{I}]$; $\begin{bmatrix} \boldsymbol{B}_1 \\ \boldsymbol{D}_{21} \end{bmatrix} \boldsymbol{D}_{21}^{\mathrm{T}} = \begin{bmatrix} \boldsymbol{0} \\ \boldsymbol{I} \end{bmatrix}$; $\mathrm{rank}\left(\boldsymbol{P}_{12}(i\omega)\right) = m_2$, $\boldsymbol{D}_{11} = \boldsymbol{D}_{22} = \boldsymbol{0}$, $\mathrm{rank}\left(\boldsymbol{P}_{21}(i\omega)\right) = p_2$, $\forall \omega \in \mathbb{R}$.

Taking into account the experimental set-up presented in **Figure 2**, we have the following set of matrices and variables to approach a H_∞ synthesis with static weights

$$\begin{gathered} \boldsymbol{C}_1 \coloneqq \begin{bmatrix} \boldsymbol{diag}(q_{z_i}) & \boldsymbol{0}_{3\times 3} \\ \boldsymbol{0}_{1\times 3} & \boldsymbol{0}_{1\times 3} \end{bmatrix};\ \boldsymbol{C}_2 \coloneqq [1 \quad 1 \quad 1 \quad 0 \quad 0 \quad 0];\ \boldsymbol{B}_1 \coloneqq \left[k_\xi \widetilde{\boldsymbol{B}}_1 \quad \boldsymbol{0}_{6\times 1}\right];\ \widetilde{\boldsymbol{B}}_1 \coloneqq \boldsymbol{B}_2; \\ \boldsymbol{D}_{11} \coloneqq [\boldsymbol{0}_{4\times 2}];\ \boldsymbol{D}_{12} \coloneqq \begin{bmatrix} \boldsymbol{0}_{3\times 1} \\ r_u \end{bmatrix};\ \boldsymbol{D}_{21} \coloneqq [0 \quad \mu_\eta];\ \boldsymbol{D}_{22} \coloneqq [0], \end{gathered} \tag{16}$$

where $\boldsymbol{x} \in \mathbb{R}^6$ is the state vector, $\boldsymbol{z} \in \mathbb{R}^4$ represents the quality output, $y \in \mathbb{R}^1$ is the measurement output, $\boldsymbol{w} = (\xi, \eta)^{\mathrm{T}} \in \mathbb{R}^2$ are the exogenous disturbances on state $\boldsymbol{x}$ and on the measured output y, respectively. $\boldsymbol{u}$ is the control vector. The constants q_{z_i}, $i = \overline{1,3}$, are weights on state z, r_u is the weight on u, μ_η is the weight on the measurement disturbance η, and k_ξ represents the weight on the state disturbance ξ. All weights are static. They can be developed as dynamics weights in an advanced scenario of robustness evaluation [29].

These equations characterize a MIMO (Multi-Input-Multi-Output) system, for which the statement of an H_∞ control problem is the following: find a controller $\boldsymbol{K}(s)$ such that $\|\boldsymbol{T}_{zw}(s)\|_\infty$ is minimized. In other words, the question is to find a controller $\boldsymbol{K}(s)$ that internally stabilizes the closed-loop system and that, given $\gamma > 0$, satisfies the condition $\|\boldsymbol{T}_{zw}\|_\infty \coloneqq \sup_{\omega \in R} \bar{\sigma}[\boldsymbol{T}_{zw}(j\omega)] < \gamma$; in other words, infinite norm of a transfer matrix $\|\boldsymbol{T}(j\omega)\|_\infty$ is defined as the supremum (minimal upper bound) of the largest singular value $\bar{\sigma}$ of its transfer matrix over the imaginary axis. A singular value of a matrix $\boldsymbol{T}(j\omega)$ is an eigenvalue of the matrix $\boldsymbol{T}^{\mathrm{T}}(-j\omega)\boldsymbol{T}(j\omega)$. A justification for the optimal H_∞ control resides in the *minimax* nature of the problem, with the argument that minimizing the "peak" of the transfer $w \to z$ necessarily renders the magnitude of $\boldsymbol{T}_{zw}$ small at all frequencies. Otherwise stated, minimizing the H_∞-norm of a transfer function is equivalent to minimizing the energy in the output signal due to the inputs with the worst possible frequency distribution. This improvement of the "worst-case scenario" has a direct correspondent in the active vibration control problem and seems particularly attractive for light structures with embedded piezoelectric actuators. The compensator is given by

$$\begin{gathered} \dot{\hat{\boldsymbol{x}}} = \widehat{\boldsymbol{A}}\hat{\boldsymbol{x}} - \boldsymbol{ZLy},\ \boldsymbol{u} = \boldsymbol{F}\hat{\boldsymbol{x}}, \\ \widehat{\boldsymbol{A}} = \boldsymbol{A} + \gamma^{-2}\boldsymbol{B}_1\boldsymbol{B}_1^{\mathrm{T}}\boldsymbol{X} + \boldsymbol{B}_2\boldsymbol{F} + \boldsymbol{ZLC}_2, \boldsymbol{F} = -\boldsymbol{B}_2^T\boldsymbol{X},\ \boldsymbol{L} = -\boldsymbol{YC}_2^T,\ \boldsymbol{Z} = (\boldsymbol{I} - \gamma^{-2}\boldsymbol{YX})^{-1} \end{gathered} \tag{17}$$

with $\boldsymbol{X}$, $\boldsymbol{Y}$ solutions of Riccati equations:

$$\begin{gathered} \boldsymbol{A}^T\boldsymbol{X} + \boldsymbol{XA} - \boldsymbol{X}(\boldsymbol{B}_2\boldsymbol{B}_2^T - \gamma^{-2}\boldsymbol{B}_1\boldsymbol{B}_1^T)\boldsymbol{X} + \boldsymbol{C}_1^T\boldsymbol{C}_1 = 0 \\ \boldsymbol{AY} + \boldsymbol{YA}^T - \boldsymbol{Y}(\boldsymbol{C}_2^T\boldsymbol{C}_2 - \gamma^{-2}\boldsymbol{C}_1^T\boldsymbol{C}_1)\boldsymbol{Y} + \boldsymbol{B}_1\boldsymbol{B}_1^T = 0. \end{gathered} \tag{18}$$

Robust H_∞ synthesis

As a robust H_∞ synthesis, the technique of assimilating the uncertainties of the mathematical model with a fictitious output-input internal reaction, see [29], [30], [31], will be used. Consider again the fundamental system (14) with the state and transfer matrix representations

$$\begin{bmatrix}\dot{\boldsymbol{x}}\\ \boldsymbol{z}\\ \boldsymbol{y}\end{bmatrix}=\begin{bmatrix}\boldsymbol{A} & \boldsymbol{B}_1 & \boldsymbol{B}_2\\ \boldsymbol{C}_1 & \boldsymbol{D}_{11} & \boldsymbol{D}_{12}\\ \boldsymbol{C}_2 & \boldsymbol{D}_{21} & \boldsymbol{D}_{22}\end{bmatrix}\begin{bmatrix}\boldsymbol{x}\\ \boldsymbol{w}\\ \boldsymbol{u}\end{bmatrix},\begin{bmatrix}\boldsymbol{z}\\ \boldsymbol{y}\end{bmatrix}=\begin{bmatrix}\boldsymbol{P}_{11} & \boldsymbol{P}_{12}\\ \boldsymbol{P}_{21} & \boldsymbol{P}_{22}\end{bmatrix}\begin{bmatrix}\boldsymbol{w}\\ \boldsymbol{u}\end{bmatrix} \tag{19}$$

The matrices are given by

$$\boldsymbol{A}=\begin{bmatrix}\boldsymbol{0}_{3\times3} & \boldsymbol{I}_3\\ \boldsymbol{diag}(-\omega_i^2) & \boldsymbol{diag}(-2\xi_i\omega_i)\end{bmatrix},\ i=\overline{1,3}.$$

$$\boldsymbol{C}_1\coloneqq\begin{bmatrix}\boldsymbol{diag}(q_i) & \boldsymbol{0}_{3\times3}\\ \boldsymbol{0}_{1\times3} & \boldsymbol{0}_{1\times3}\end{bmatrix};\ \boldsymbol{C}_2\coloneqq[1\quad 1\quad 1\quad 0\quad 0\quad 0];\ \boldsymbol{B}_1\coloneqq\begin{bmatrix}k_\xi\widetilde{\boldsymbol{B}}_1 & \boldsymbol{0}_{6\times1}\end{bmatrix};\ \widetilde{\boldsymbol{B}}_1\coloneqq\boldsymbol{B}_2; \tag{20}$$

$$\boldsymbol{D}_{11}\coloneqq[\boldsymbol{0}_{4\times2}];\ \boldsymbol{D}_{12}\coloneqq\begin{bmatrix}\boldsymbol{0}_{3\times1}\\ r_u\end{bmatrix};\ \boldsymbol{D}_{21}\coloneqq\begin{bmatrix}0 & \mu_\eta\end{bmatrix};\ \boldsymbol{D}_{22}\coloneqq[0];$$

Weights were taken from the standard H_∞ synthesis. Consider the perturbed system:

$$\begin{bmatrix}\dot{\boldsymbol{x}}\\ \boldsymbol{z}\\ \boldsymbol{y}\end{bmatrix}=\left(\begin{bmatrix}\boldsymbol{A} & \boldsymbol{B}_1 & \boldsymbol{B}_2\\ \boldsymbol{C}_1 & \boldsymbol{D}_{11} & \boldsymbol{D}_{12}\\ \boldsymbol{C}_2 & \boldsymbol{D}_{21} & \boldsymbol{D}_{22}\end{bmatrix}+\boldsymbol{\Delta}\right)\begin{bmatrix}\boldsymbol{x}\\ \boldsymbol{w}\\ \boldsymbol{u}\end{bmatrix};\boldsymbol{\Delta}\coloneqq\begin{bmatrix}\boldsymbol{\Delta A} & 0 & 0\\ 0 & 0 & 0\\ 0 & 0 & 0\end{bmatrix}. \tag{21}$$

Evaluating the values of the transfer functions from Table 1, it can be seen that the damping ratios are the most susceptible to uncertainty, being at the same time the most important for the oscillatory nature of the wing structure. In this situation, let introduce the factorization:

$$\boldsymbol{\Delta A}=-\boldsymbol{M}_x\boldsymbol{E}\boldsymbol{N}_x,\ \boldsymbol{E}=\boldsymbol{diag}(\delta_i),\ i=\overline{1,3}. \tag{22}$$

Therefore, the perturbation δ_i was introduced as $\zeta_i\to\zeta_i+\delta_i,\ i=\overline{1,3}$, thus the matrix $\boldsymbol{\Delta A}$ has the following form:

$$\boldsymbol{\Delta A}=\begin{bmatrix}\boldsymbol{0}_{3\times3} & \boldsymbol{0}_{3\times3}\\ \boldsymbol{0}_{3\times3} & \boldsymbol{diag}(-2\zeta_i\delta_i)\end{bmatrix},\ i=\overline{1,3}. \tag{23}$$

The matrices $\boldsymbol{M}_x,\ \boldsymbol{E},\ \boldsymbol{N}_x$ are:

$$\boldsymbol{M}_x=\begin{bmatrix}\boldsymbol{0}_{3\times3}\\ \boldsymbol{I}_3\end{bmatrix};\ \boldsymbol{E}=\boldsymbol{diag}(\delta_i);\ \boldsymbol{N}_x=[\boldsymbol{0}_{3\times3}\quad\boldsymbol{diag}(-2\omega_i)],\ i=\overline{1,3}. \tag{24}$$

New fictitious input and output, $\tilde{\boldsymbol{z}}$ and $\widetilde{\boldsymbol{w}}$, are introduced

$$\tilde{\boldsymbol{z}}\coloneqq\boldsymbol{N}_x\boldsymbol{x},\ \widetilde{\boldsymbol{w}}=-\boldsymbol{E}\tilde{\boldsymbol{z}}. \tag{25}$$

The system extended with state and transfer matrices is given by:

$$\begin{bmatrix}\dot{\boldsymbol{x}}\\ \tilde{\boldsymbol{z}}\\ \boldsymbol{z}\\ \boldsymbol{y}\end{bmatrix}=\begin{bmatrix}\boldsymbol{A} & \boldsymbol{M}_x & \boldsymbol{B}_1 & \boldsymbol{B}_2\\ \boldsymbol{N}_x & \boldsymbol{0}_{3\times3} & \boldsymbol{0}_{3\times2} & \boldsymbol{0}_{3\times1}\\ \boldsymbol{C}_1 & \boldsymbol{0}_{4\times3} & \boldsymbol{D}_{11} & \boldsymbol{D}_{12}\\ \boldsymbol{C}_2 & \boldsymbol{0}_{1\times3} & \boldsymbol{D}_{21} & \boldsymbol{D}_{22}\end{bmatrix}\begin{bmatrix}\boldsymbol{x}\\ \widetilde{\boldsymbol{w}}\\ \boldsymbol{w}\\ \boldsymbol{u}\end{bmatrix};\begin{bmatrix}\tilde{\boldsymbol{z}}\\ \boldsymbol{z}\\ \boldsymbol{y}\end{bmatrix}=\begin{bmatrix}\boldsymbol{G}_{11} & \boldsymbol{G}_{12} & \boldsymbol{G}_{13}\\ \boldsymbol{G}_{21} & \boldsymbol{G}_{22} & \boldsymbol{G}_{23}\\ \boldsymbol{G}_{31} & \boldsymbol{G}_{32} & \boldsymbol{G}_{33}\end{bmatrix}\begin{bmatrix}\widetilde{\boldsymbol{w}}\\ \boldsymbol{w}\\ \boldsymbol{u}\end{bmatrix}. \tag{26}$$

The new perturbed system, that contains the fictitious variables, is:

$$\dot{\boldsymbol{x}} = \boldsymbol{A}\boldsymbol{x} + \boldsymbol{B}_1\hat{\boldsymbol{w}} + \boldsymbol{B}_2\boldsymbol{u};\ \hat{\boldsymbol{z}} = \boldsymbol{C}_1\boldsymbol{x} + \boldsymbol{D}_{11}\hat{\boldsymbol{w}} + \boldsymbol{D}_{12}\boldsymbol{u}, \boldsymbol{y} = \boldsymbol{C}_2\boldsymbol{x} + \boldsymbol{D}_{21}\hat{\boldsymbol{w}} + \boldsymbol{D}_{22}\boldsymbol{u} \tag{27}$$

with the following notation:

$$\hat{\boldsymbol{z}} = \begin{bmatrix}\tilde{\boldsymbol{z}}\\ \boldsymbol{z}\end{bmatrix};\ \hat{\boldsymbol{w}} = \begin{bmatrix}\widetilde{\boldsymbol{w}}\\ \boldsymbol{w}\end{bmatrix};\ \boldsymbol{C}_1 = \begin{bmatrix}\boldsymbol{N}_x\\ \boldsymbol{C}_1\end{bmatrix};$$
$$\boldsymbol{D}_{11} = \begin{bmatrix}\boldsymbol{0}_{3\times3} & \boldsymbol{0}_{3\times2}\\ \boldsymbol{0}_{4\times3} & \boldsymbol{D}_{11}\end{bmatrix};\ \boldsymbol{D}_{12} = \begin{bmatrix}\boldsymbol{0}_{3\times1}\\ \boldsymbol{D}_{12}\end{bmatrix}; \boldsymbol{D}_{21} = [\boldsymbol{0}_{1\times3} \quad \boldsymbol{D}_{21}]; \boldsymbol{B}_1 = [\boldsymbol{M}_x \quad \boldsymbol{B}_1]. \tag{28}$$

After the synthesis of the compensator$\boldsymbol{K}(s)$, the closed loop transfer $\hat{\boldsymbol{w}} \to \hat{\boldsymbol{z}}$ is obtained as $\hat{\boldsymbol{z}} = \boldsymbol{T}_{\hat{z}\hat{w}}\hat{\boldsymbol{w}}, \boldsymbol{T}_{\hat{z}\hat{w}} = \begin{bmatrix}\boldsymbol{T}_{11} & \boldsymbol{T}_{12}\\ \boldsymbol{T}_{21} & \boldsymbol{T}_{22}\end{bmatrix}$ with

$$\boldsymbol{T}_{11} = \boldsymbol{G}_{11} - \boldsymbol{G}_{13}\boldsymbol{K}(\boldsymbol{I} + \boldsymbol{G}_{33}\boldsymbol{K})^{-1}\boldsymbol{G}_{31};\ \boldsymbol{T}_{12} = \boldsymbol{G}_{12} - \boldsymbol{G}_{13}\boldsymbol{K}(\boldsymbol{I} + \boldsymbol{G}_{33}\boldsymbol{K})^{-1}\boldsymbol{G}_{32}$$
$$\boldsymbol{T}_{21} = \boldsymbol{G}_{21} - \boldsymbol{G}_{23}\boldsymbol{K}(\boldsymbol{I} + \boldsymbol{G}_{33}\boldsymbol{K})^{-1}\boldsymbol{G}_{31};\ \boldsymbol{T}_{22} = \boldsymbol{G}_{22} - \boldsymbol{G}_{23}\boldsymbol{K}(\boldsymbol{I} + \boldsymbol{G}_{33}\boldsymbol{K})^{-1}\boldsymbol{G}_{32}. \tag{29}$$

We must bear in mind that the actual transfer is

$$\boldsymbol{T}_{zw} = \boldsymbol{T}_{22} - \boldsymbol{T}_{21}\boldsymbol{E}(\boldsymbol{I} + \boldsymbol{T}_{11}\boldsymbol{E})^{-1}\boldsymbol{T}_{12}. \tag{30}$$

The following theorems [31] provide sufficient conditions for stability/performance robustness.

Theorem 1 (stability robustness). *If* $\|\boldsymbol{T}_{11}(s)\|_\infty < \gamma$, *then* $\boldsymbol{T}_{zw}(s, \alpha\boldsymbol{E})$, $\forall\alpha \in [0,1]$, *is stable for* $\|\boldsymbol{E}\| \le \gamma^{-1}$.

Theorem 2 (performance robustness.) *If* $\|\boldsymbol{T}_{\hat{z}\hat{w}}\|_\infty < \gamma$, *then* $\boldsymbol{T}_{zw}(s, \alpha\boldsymbol{E})$, $\forall\alpha \in [0,1]$, *is stable and* $\|\boldsymbol{T}_{zw}(s, \alpha\boldsymbol{E})\|_\infty < \gamma$, $\forall\alpha \in [0,1]$ *and* $\|\boldsymbol{E}\| \le \gamma^{-1}$.

The following theorem gives a robust H_∞ suboptimal controller that satisfies the condition of Theorem 2.

Theorem 3. *Assume that* (A1) $(\boldsymbol{A}, \boldsymbol{B}_2)$ is *stabilizable and* $(\boldsymbol{C}_2, \boldsymbol{A})$ is *detectable;* (A2) $\boldsymbol{D}_{12}^{\mathrm{T}}[C_1 \quad \boldsymbol{D}_{12}] = [\boldsymbol{0} \quad \boldsymbol{I}]$ *and* $\begin{bmatrix}\boldsymbol{B}_1\\ \boldsymbol{D}_{21}\end{bmatrix}\boldsymbol{D}_{21}^{\mathrm{T}} = \begin{bmatrix}\boldsymbol{0}\\ \boldsymbol{I}\end{bmatrix}$; (A3) $\mathrm{rank}\big(\boldsymbol{P}_{12}(i\omega)\big) = 1$, $\mathrm{rank}\big(\boldsymbol{P}_{21}(i\omega)\big) = 1$, $\forall\omega \in \mathbb{R}$; (A4) $\boldsymbol{D}_{11} = \boldsymbol{D}_{22} = 0$.
The internal stabilizing compensator that provides $\|\boldsymbol{T}_{\hat{z}\hat{w}}\|_\infty < \gamma$ *exists if and only if the Riccati equations*

$$\boldsymbol{A}^{\mathrm{T}}\boldsymbol{X} + \boldsymbol{X}\boldsymbol{A} - \boldsymbol{X}\big(\boldsymbol{B}_2\boldsymbol{B}_2^{\mathrm{T}} - \gamma^{-2}\boldsymbol{B}_1\boldsymbol{B}_1^{\mathrm{T}}\big)\boldsymbol{X} + \boldsymbol{C}_1^{\mathrm{T}}\boldsymbol{C}_1 = 0$$
$$\boldsymbol{A}\boldsymbol{Y} + \boldsymbol{Y}\boldsymbol{A}^{\mathrm{T}} - \boldsymbol{Y}\big(\boldsymbol{C}_2^{\mathrm{T}}\boldsymbol{C}_2 - \gamma^{-2}\boldsymbol{C}_1^{\mathrm{T}}\boldsymbol{C}_1\big)\boldsymbol{Y} + \boldsymbol{B}_1\boldsymbol{B}_1^{\mathrm{T}} = 0 \tag{31}$$

have symmetric, stabilizing solutions $\boldsymbol{X} \ge 0,\ \boldsymbol{Y} \ge 0$ (i.e., $\boldsymbol{A} - \big(\boldsymbol{B}_2\boldsymbol{B}_2^{\mathrm{T}} - \gamma^{-2}\boldsymbol{B}_1\boldsymbol{B}_1^{\mathrm{T}}\big)\boldsymbol{X}$ *and* $\boldsymbol{A} - \boldsymbol{Y}\big(\boldsymbol{C}_2^{\mathrm{T}}\boldsymbol{C}_2 - \gamma^{-2}\boldsymbol{C}_1^{\mathrm{T}}\boldsymbol{C}_1\big)$ *are stable matrices*) *and* $(\boldsymbol{I} - \gamma^{-2}\boldsymbol{Y}\boldsymbol{X})\boldsymbol{Y} \ge 0$. *The compensator (suboptimal one), is given by*:

$$\boldsymbol{K} = \left[\begin{array}{c|c}\widehat{\boldsymbol{A}} & -\boldsymbol{Z}\boldsymbol{L}\\ \hline \boldsymbol{F} & 0\end{array}\right] \tag{32}$$

with:

$$\widehat{\boldsymbol{A}} := \boldsymbol{A} + \gamma^{-2}\boldsymbol{B}_1\boldsymbol{B}_1^{\mathrm{T}}\boldsymbol{X} + \boldsymbol{B}_2\boldsymbol{F} + \boldsymbol{Z}\boldsymbol{L}\boldsymbol{C}_2,\ \boldsymbol{F} := -\boldsymbol{B}_1^{\mathrm{T}}\boldsymbol{X},\ \boldsymbol{L} := -\boldsymbol{Y}\boldsymbol{C}_2^{\mathrm{T}},\ \boldsymbol{Z} := (\boldsymbol{I} - \gamma^{-2}\boldsymbol{Y}\boldsymbol{X})^{-1}. \tag{33}$$

Remark. The assertion in Section 1 "*The compatibility between a mathematical methodology intended to be used for control law synthesis and the mathematical model to which this methodology is applied" can be better understood if we refer only to Theorem 3, in which a set of constraints (A1) - (A4) conditions the application of the synthesis method to the mathematical model (19).*

3. NUMERICAL ANALYSIS OF THE ROBUSTNESS PERFORMANCES OF THE COMPENSATORS AND CONCLUSIONS

As was mentioned in the beginning of this paper, four air velocities in the WT were chosen for the experiment with the wing demonstrator for vibration attenuation, specifically for flutter mitigation: $V_1 = 15$ m/s; $V_2 = 20$ m/s; $V_3 = 25$ m/s; $V_4 = 30$ m/s.

The numerical transfer functions $u \to y_1$ for the four velocities were obtained by experimental identification and subsequently, by using the IDTOOL identification procedures in MATLAB/ Simulink, rational analytical expressions in frequency domain needed in the control synthesis were deduced.

Finally, from the expressions in the frequency domain, the state realizations in time domain were derived.

For example, for $V_4 = 30$ m/s, the identified matrices are:

$$\boldsymbol{A} = \begin{bmatrix} 0 & 0 & 0 & 1 & 0 & 0 \\ 0 & 0 & 0 & 0 & 1 & 0 \\ 0 & 0 & 0 & 0 & 0 & 1 \\ -1427 & 0 & 0 & -3.38 & 0 & 0 \\ 0 & -9021 & 0 & 0 & -27.84 & 0 \\ 0 & 0 & -53345 & 0 & 0 & -162.9 \end{bmatrix}; \boldsymbol{B}_2 = \begin{bmatrix} 0.282 \\ -0.231 \\ -0.051 \\ 78.62 \\ -176.62 \\ 103.2 \end{bmatrix} \quad (34)$$

The control law strategy was thought as follows: choose the law associated with a velocity, namely velocity V_2, and test its robustness when applied in the context of velocities V_1, V_3, V_4.

Any other combination can be analysed, in principle, for a possible optimization.

Analysis of the system with LQG and LQG/LTR compensators

The LQG active control and some illustrative numerical simulations are based on relations (3)-(11).

The parameters used in simulations are: $\boldsymbol{C}_2 = [1 \quad 1 \quad 1 \quad 0 \quad 0 \quad 0]$; $\boldsymbol{C}_1 = \boldsymbol{C}_2$, $\boldsymbol{B}_1 = \boldsymbol{B}_2$; $Q_\xi = 1$; $Q_\eta = 10^{-5}$; $\mu = 1$; $\rho = 0.15$; $q = 10^6$; $R = 0.2$; $\boldsymbol{Q} = \boldsymbol{C}_1^{\mathrm{T}} \boldsymbol{Q}_j \boldsymbol{C}_1 = \boldsymbol{diag}[5 \quad 5 \quad 0 \quad 0 \quad 0 \quad 0]$.

The controller LQG corresponding to V_2 was also used for the other speeds V_1, V_3, V_4 and denotes a remarkable robustness (**Figure 2**).

The attenuations of base frequency on the four air velocities V_1, V_2, V_3, V_4 are 5.46 dB, 6.99 dB, 8.06 dB and 8.42 dB, respectively.

Unfortunately, the system $(\boldsymbol{C}_2, \boldsymbol{A}, \boldsymbol{B}_2, \boldsymbol{0})$ is not of minimum phase, therefore the LQG/LTR procedure is not rigorous in recovering the robustness of the LQR regulator.

However, the recommendation in the paper [25] was taken into account and the LQG/LTR synthesis procedure as described in **Proposition 2** was continued up to a value of $q = 10^6$. Surprisingly, the LQG/LTR V_2 regulator thus provided is proving to be also robust, as shown in **Figure 3**.

As expected, slightly better attenuations are obtained on the base frequency, on the four air velocities V_1, V_2, V_3, V_4: 5.52 dB, 7.06 dB, 8.13 dB and 8.54 dB, respectively.

Forcing greater control by lowering R to 0.05 is not desirable, as the first two frequencies approach each other at V_4, which increases the risk of flutter (**Figure 4**) [13]. However, it should be noted that the LQG/LTR procedure, even if it is mathematically legitimate, is not infallible [3].

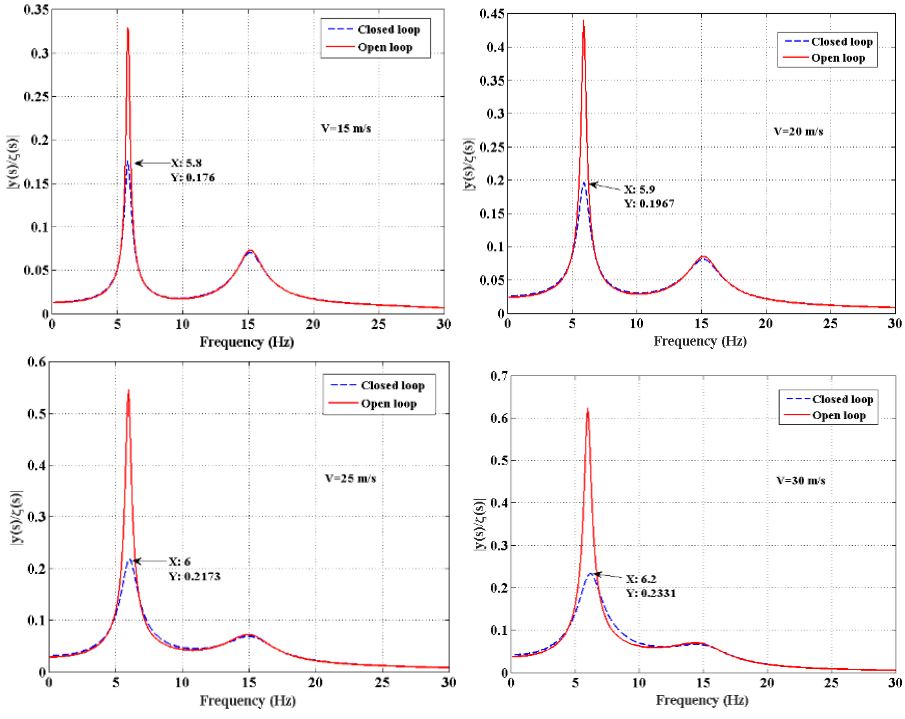

Figure 2 – LQG synthesis. Robustness of V_2 reference compensator

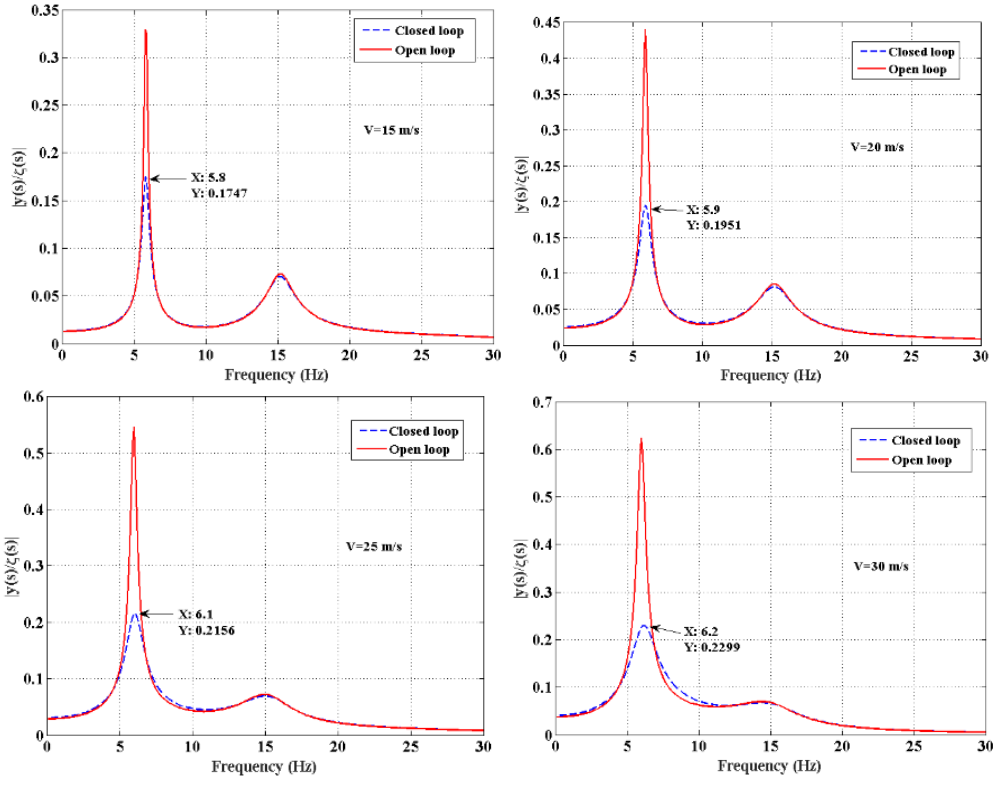

Figure 3 – LQG/LTR synthesis. Robustness of V_2 reference compensator

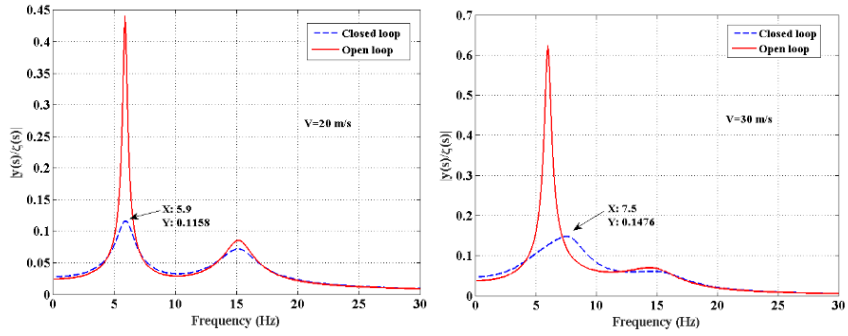

Figure 4 – Forcing a stronger attenuation by increasing the control leads to harmful shifting of the base frequency

Let's remember that $\boldsymbol{S}(s)$ must be small whenever output perturbations are large and $\boldsymbol{T}(s)$ must be small whenever model errors are large. In **Figure 5** the graph on the left describes the performance in the presence of disturbances of the nominal compensator LQG/LTR V_2 designed for a stronger attenuation (**Figure 4**) and the one on the right is associated with the same type of compensator, but slightly relaxed (**Figure 3**). For at least two reasons, the last compensator is preferable: maintaining the distance between the resonance peaks and better management of modelling errors.

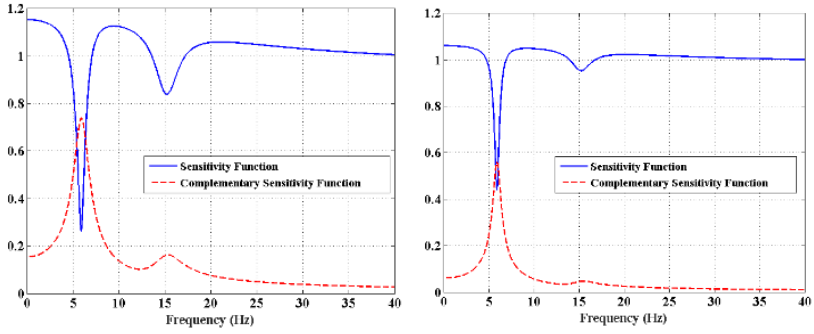

Figure 5 – Functions ***S***(s) and ***T***(s) for two LQG/LTR V_2 compensators, the one on the right with relatively more moderate attenuations

On the top of **Figure 6**, on the left, it is shown the extent to which the structure of the LQG/LTR compensator approached the structure of robust LQR compensator, based on **Propositions 1 and 2**. On the right, it is shown a numerical simulation from which one can see the strong vibration damping when the control comes into action. On the bottom of **Figure 6,** one can see a slight increase in the robustness of the LQG/LTR compensator compared to the LQG compensator.

Analysis of the system with H_∞ and robust H_∞ compensators

Synthesis parameters of the standard H_∞ compensator were chosen by trial and error procedure: $q_{z_1} = 3;\ q_{z_2} = 10;\ q_{z_3} = 0.01;\ r_u = 1; k_\xi = 1;\ \mu_\eta = 0.01$. In the case of robust H_∞ compensator the following parameters were chosen $k_\xi = 0.001,\ q_{z_1} = 10;\ q_{z_2} = 1;\ q_{z_3} = 0.01;\ r_u = 0.1;\ \mu_\eta = 0.0035$.

Representative results are summarized in **Figures 7 and 8**. For the standard H_∞ compensator, the attenuations of base frequency on the four air velocities V_1, V_2, V_3, V_4 are 6.88 dB, 8.53 dB, 9.52 dB and 9.41 dB, respectively. For the robust H_∞ compensator, the

attenuations of base frequency on the four air velocities V_1, V_2, V_3, V_4 are 8.65 dB, 10.35 dB, 11.38 dB and 11.48 dB respectively. In conclusion, the robust H_∞ compensator developed in this paper proves to be the most efficient. It is worth mentioning the γ value provided by the H_∞ synthesis solving the Riccati equations for the extended system with fictitious input-output, $\|\boldsymbol{T}_{11}(s)\|_\infty = 12.629 < \gamma = 12.78$ and $\|\boldsymbol{T}_{\hat{z}\hat{w}}\|_\infty = 12.63 < \gamma$. The values obtained for the two norms attest the conditions fulfilment of **Theorems 1 and 2** of stability robustness, and performance robustness, respectively.

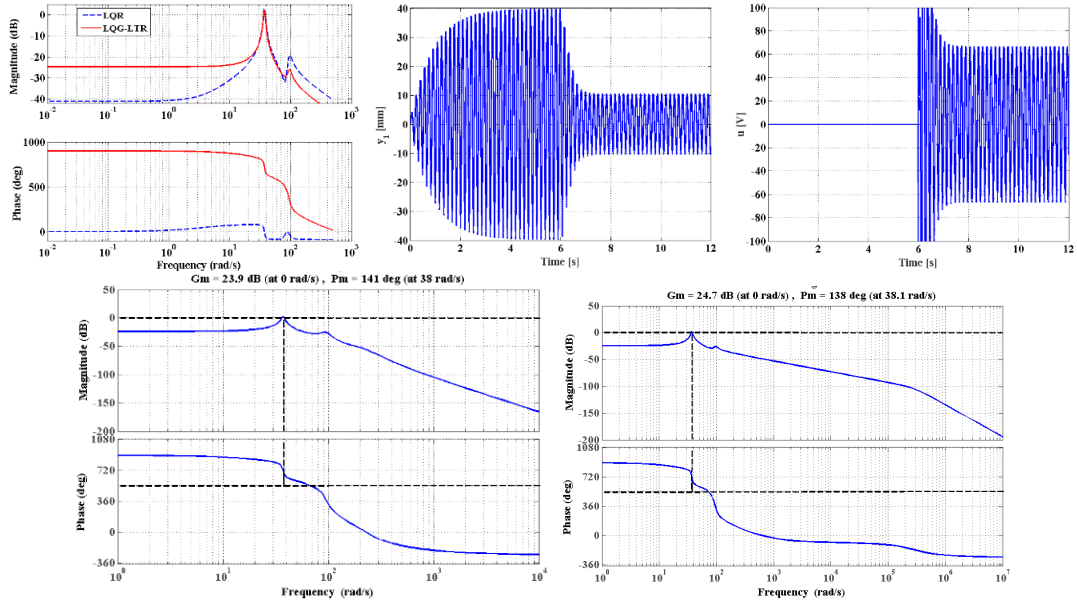

Figure 6 – Top figures: Bode comparison LQR versus LQG/LTR and LQG/LTR time histories for nominal compensator V_2; bottom figures: stability margins LQG versus LQG/LTR for V_2 compensator; an increase in the stability reserve of the LQG /LTR (right) compensator can be observed

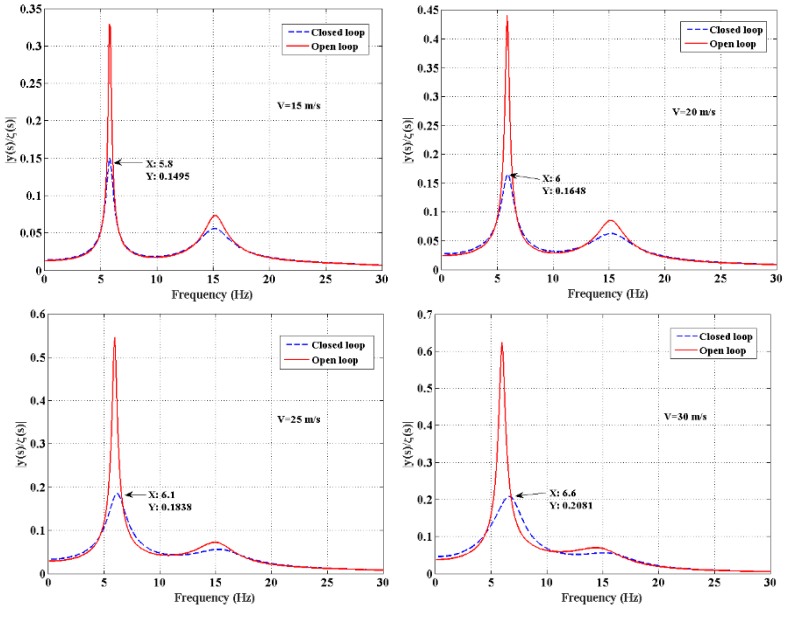

Figure 7 – Performance of standard H_∞ V_2 compensator

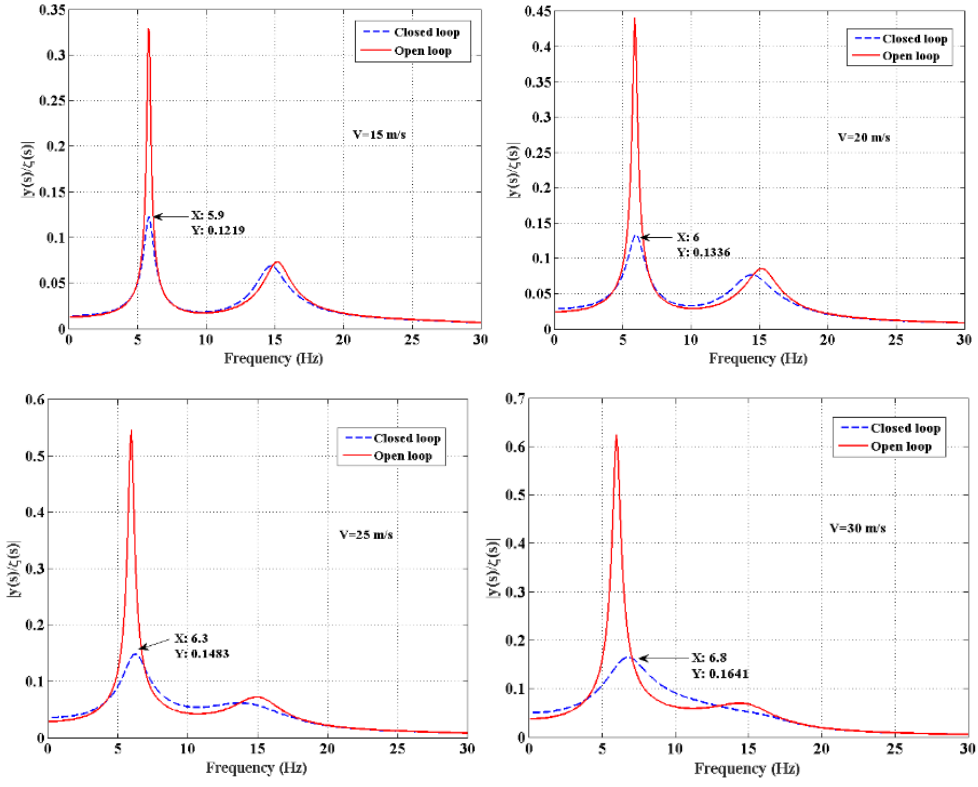

Figure 8 – Performance of robust H_∞ V_2 compensator

The results of this work continue a long experience of the authors in the field of applied control [1-4, 8-10, 14, 16-18, 32-40]. Any approach is effective, provided that the synthesis methodology is compatible with the mathematical model. Obviously, the research cycle will end with the implementation and validation of the methodology on the smart wing.

ACKNOWLEDGMENTS

This work was supported by a grant of the Romanian Ministry of Research and Innovation, CCCDI – UEFISCDI, project number 87PCCDI/2018, project registration code PN-III-P1-1.2-PCCDI-2017-0868, within PNCDI III.

REFERENCES

[1] I. Ursu, The kinematics of the rigid feedback linkage, the impedance of the hydraulic servomechanism and the flutter occurrence, *INCAS Bulletin*, vol. **4**, no. 3, pp. 63-70, http://dx.doi.org/10.13111/2066-8201.2012.4.3.6, 2012.

[2] I. Ursu, M. Vladimirescu, F. Ursu, About aeroservoelasticity criteria for electrohydraulic servomechanisms synthesis, *Proceedings of the 20th Congress of the International Council of the Aeronautical Sciences, ICAS 96*, vol. **2**, pp. 2335-2344, 1996.

[3] I. Ursu, F. Ursu, *Active and semiactive control (Romanian)*, Publishing House of the Romanian Academy, Bucharest, 2002.

[4] I. Ursu, Study of the stability and compatibility of the hydraulic servomechanisms from the primary flight controls (in Romanian), *Internal report IMFCA-INCAS, code 34125*, 1974.

[5] E. Livne, Aircraft Active Flutter Suppression: State of the Art and Technology Maturation Needs, *Journal of Aircraft*, vol. **55**, no. 1, pp. 410-450, 2018.

[6] L. W. Trame, L.E. Williams, R. N. Yurkovich, Active aeroelastic oscillation control on the F/A-18 Aircraft, *AIAA Guidance Navigation and Control Conference*, 1985.
[7] Y. M. Ram, J. E. Mottershead, Receptance method in active vibration control, *American Institute of Aeronautics and Astronautics Journal*, vol. **45**, no. 3, pp. 562-567, 2007.
[8] I. Ursu, D. D. Ion Guta, D. Enciu, G. Tecuceanu, A. A. Radu, Flight envelope expansion based on active mitigation of flutter via a V-stack piezoelectric actuator, *IOP Conference Series. Journal of Physics: Conference Series*, vol. **1106**, pp. 012033, 2018.
[9] D. Enciu, I. Ursu, G. Tecuceanu, D. D. Ion Guta, A. Halanay, M. Tudose, Flight envelope expansion via piezoelectric actuation. Receptance method and time-delayed feedback control, *International Journal of Modelling and Optimization*, vol. **9**, no. 6, pp. 317-321, 2019.
[10] I. Ursu, D. D. Ion Guta, D. Enciu, A. Toader, M. Dan, C. Donciu, V. Turcan, Mathematical modelling of a V-stack piezoelectric aileron actuation, *INCAS Bulletin*, vol. **8**, no. 4, pp. 141-155, http://dx.doi.org/10.13111/2066-8201.2016.8.4.12, 2016.
[11] F. Munteanu, C. Oprean, C. Stoica, INCAS Subsonic Wind Tunnel, *INCAS Bulletin*, vol. **1**, pp. 12-14, http://dx.doi.org/10.13111/2066-8201.2009.1.1.3, 2009.
[12] E. V. Ardelean, M. A. McEver, D. G. Cole, R. L. Clark, Active flutter control with V-stack piezoelectric flap actuator, *Journal of Aircraft*, vol. **43**, no. 2, pp. 482-486, 2006.
[13] E. Papatheou, N. D. Tantaroudas, A. Da Ronch, J. E. Cooper, J. E. Mottershead, *Active control for flutter suppression: an experimental investigation*, In International Forum on Aeroservoelasticity and Structural Dynamics (IFASD), United Kingdom, 2013.
[14] I. Ursu, F. Ursu, F. Popescu, Backstepping design for controlling electrohydraulic servos, *Journal of the Franklin Institute*, vol. **343**, pp. 94-110, 2006.
[15] B. Xu, W. Zhang, J. Ma, Stability and Hopf bifurcation of a two-dimensional supersonic airfoil with a time-delayed feedback control surface, *Nonlinear Dynamics*, vol. **77**, pp. 819-837, 2014.
[16] L. Iorga, H. Baruh, I. Ursu, H_∞ control with μ-analysis of a piezoelectric actuated plate, *Journal of Vibration and Control*, vol. **15**, no. 8, pp. 1143-1171, 2009.
[17] E. Munteanu, I. Ursu, Active control techniques for piezo smart composite wing, *Proceedings of the 9th WSEAS International Conference on Automation and Information (ICAI '08)*, pp.554-559, 2008.
[18] I. Ursu, L. Iorga, A. Toader, G. Tecuceanu, *Active Robust Control of a Smart Plate*, ICINCO 2011 8th International Conference on Informatics in Control, Automation and Robotics, Noordwijkerhout, The Netherlands, 2011.
[19] H. Kwakernaak, R. Sivan, *Linear Optimal Control Systems*, Wiley-Interscience; 1972.
[20] R. E. Kalman, Contributions to the theory of optimal control, *Boletín de la Sociedad Matemática Mexicana*, vol. **5**, pp. 102-109, 1960.
[21] J. C. Doyle, Guaranteed margins for LQG regulators, *IEEE Transactions on Automatic Control*, vol. **AC-23**, no. 4, pp. 756-757, 1978.
[22] J. C. Doyle, G. Stein, Robustness with observers, *IEEE Transactions on Automatic Control*, vol. **24**, pp. 607-611, 1979.
[23] C. B. Schrader, M. K. Sain, Research on system zeros: a survey, *International Journal on Control*, vol. **50**, no. 4, pp. 1407-1433, 1989.
[24] E. J. Davidson, Some properties of minimum phase systems and "squared-down" systems, *IEEE Transactions on Automatic Control*, vol. **AC-28**, no. 2, pp. 221-222, 1983.
[25] G. Stein, M. Athans, The LQG/LTR procedure for multivariable feedback control design, *IEEE Transactions on Automatic Control*, vol. **AC-32**, no. 2, pp. 105-114, 1987.
[26] I. Postlethwaite, S. Skogestad, *Robust multivariable control using H_∞ methods: analysis, design and industrial applications*, in H. L. Trentelman and J. C. Willems (Eds.) *Essays on Control - Perspectives in the Theory and its Applications*, pp. 269-337, Birkhäuser, 1993.
[27] J. C. Doyle, G. Stein, Multivariable feedback design: concepts for a classical/modern synthesis, *IEEE Transactions on Automatic Control*, vol. **46**, no. 1, pp. 4-16, 1981.
[28] K. Zhou, J. C. Doyle, K. Glover, *Robust and optimal control*, Prentice Hall, 1996.
[29] M. Tahk, J. L. Speyer, Modelling of parameter variations and asymptotic LQG synthesis, *IEEE Transactions on Automatic Control*, vol. **32**, no. 9, pp. 793-801, 1987.
[30] K. W. Byun, B. Wie, D. Geller, J. Sunkel, Robustified H_∞ control design for the space station with structured parameter uncertainty, *Journal of Guidance, Control and Dynamics*, vol. **14**, no. 6, pp. 1115-1122, 1991.
[31] B. Wie, L. Qiang, K. W. Byun, Robust control synthesis method and its application to benchmark problems, *Journal of Guidance, Control and Dynamics*, vol. **15**, no. 5, pp. 1140-1148, 1992.
[32] I. Ursu, Dealing with mathematical modeling in applied control, *INCAS Bulletin*, vol. **3**, no. 2, pp. 87-93, http://dx.doi.org/10.13111/2066-8201.2011.3.2.9, 2011.

[33] A. Toader, I. Ursu, Pilot modelling based on time delay synthesis, *Proceedings of the Institution of Mechanical Engineers – Part G: Journal of Aerospace Engineering*, vol. **228**, no. 5, pp. 740-754, 2014.
[34] * * * PN-II-PT-PCCA-2013-4-2006, *Antiflutter demonstrator with piezolectric actuator*, National Research Contract no. 289/2014.
[35] I. Ursu, D. Enciu, G. Tecuceanu, Equilibrium stability of a nonlinear structural switching system with actuator delay, *Journal of the Franklin Institute*, vol. **357**, no. 6, pp.3680-370, 2020.
[36] * * * PN-III-P1-1.2-PCCDI-2017-086, *Emerging technologies to counteract the effects induced by the turbulent flows of fluid media*, 2018-2021.
[37] I. Ursu, G. Tecuceanu, D. Enciu, A. Toader, M. Arghir, *A smart wing model: from designing to testing in wind tunnel with turbulence generator*, submitted.
[38] D. Enciu, A. Halanay, Stability for a delayed switched nonlinear system of differential equations in a critical case, *International Journal of Control*, https://doi.org/10.1080/00207179.2020.1862423, 2021.
[39] D. Enciu, A. Halanay, A. Toader, I. Ursu, *Lyapunov-Malkin type approach of equilibrium stability in a critical case applied to a switched model of a servomechanism with state delay*, submitted.
[40] D. D. Ion-Guţă, I. Ursu, A. Toader, D. Enciu, P. A. Dancă, I. Năstase, C. V. Croitoru, F. I. Bode, M. Sandu, Advanced thermal manikin for thermal comfort assessment in vehicles and buildings, *Applied Sciences,* 2022.